Integrated Photonic Electromagnetic Field Sensor Based on Broadband Bowtie Antenna Coupled Silicon Organic Hybrid Modulator

Xingyu Zhang, *Student Member, IEEE*, Amir Hosseini, Harish Subbaraman, Shiyi Wang, Qiwen Zhan, Jingdong Luo, Alex K.-Y. Jen, and Ray T. Chen

Abstract—We present the design, fabrication and characterization of a compact and highly sensitive integrated photonic electromagnetic field sensor based on a silicon-organic hybrid modulator driven by a bowtie antenna. Slow-light effects in the electro-optic (EO) polymer refilled silicon slot photonic crystal waveguide (PCW), together with broadband electric field enhancement provided by the bowtie antenna, are utilized to enhance the interaction of microwaves and optical waves, enabling an ultra large effective in-device EO coefficient over 1000 pm/V and thus a high sensitivity. The EO polymer refilled slot PCW is designed for low-dispersion slow-light propagation, high poling efficiency, and high optical mode confinement inside the slot. The bowtie antenna acts not only as a receiving antenna, but also as poling electrodes during the fabrication process. A bowtie antenna integrated on doped silicon slot PCW is demonstrated to have a broad operational bandwidth, with a maximum resonance at the frequency of 10 GHz. The strongly enhanced broadband electric field is used to directly modulate the phase of the optical waves propagating through the slot PCW embedded inside the feed gap of the bowtie antenna. The phase modulation is then converted to intensity modulation using an external reference arm to form a Mach-Zehnder interferometer in our experimental setup. The sensing of electromagnetic field at 8.4 GHz is experimentally demonstrated, with a minimum detectable electromagnetic power density of $8.4\,\mathrm{mW/m^2}$, corresponding to a minimum detectable electric field of 2.5 V/m.

Index Terms—Antennas, electromagnetic fields, electrooptic modulators, integrated optics, microwave photonics, optical sensors, photonic crystals, polymers, silicon photonics, slow light.

X. Zhang and R. T. Chen are with the Microelectronic Research Center, Department of Electrical and Computer Engineering, University of Texas, Austin, TX 78758 USA (e-mail: xzhang@utexas.edu; raychen@uts.cc.utexas.edu).

A. Hosseini and H. Subbaraman are with Omega Optics, Inc., Austin, TX 78757, USA (e-mail: amir.hosseini@omegaoptics.com; harish.subbaraman@omegaoptics.com).

S. Wang and Q. Zhan are with Electro-Optics Program, Department of Electrical & Computer Engineering, University of Dayton, Dayton, OH 45469-2951 USA (e-mail: sywang.opt@gmail.com; qzhan1@udayton.edu).

J. Luo and A. K.-Y. Jen are with The Department of Material Science and Engineering, University of Washington, Seattle, WA 98195 USA (e-mail: jdluo@uw.edu; ajen@uw.edu).

Color versions of one or more of the figures in this paper are available online at http://ieeexplore.ieee.org.

I. INTRODUCTION

THE detection, measurement and evaluation of electromagnetic fields have attracted a significant amount of attention in recent years [1]–[3]. Electromagnetic field sensors have shown promising applications in high power microwave and electromagnetic pulse detection, environmental electromagnetic interference analysis, electromagnetic compatibility measurements, radio frequency (RF) integrated circuit testing, process monitoring and control, as well as in the research of electromagnetic radiation effects on human health. Traditional electronic-based electromagnetic field sensors [4], [5] normally have large active conductive probes which perturb the field to be measured and also make the device bulky. In order to address these problems, integrated photonic sensing of electromagnetic field has been developed, in which the optical signal is modulated by an RF signal collected by an antenna [6]–[11]. The antennas used here can potentially be designed to be small enough or all-dielectric [12] to minimize the perturbation of high-frequency electric field under measurement. The key element of such devices is an efficient electro-optic (EO) modulator. One common structure of EO modulators is a Mach-Zehnder interferometer (MZI), in which an electric-field-induced optical phase modulation is converted into an optical intensity variation [13], [14]. These integrated photonic electromagnetic field sensors have a few inherent advantages over conventional electronic sensors, such as compact size, high sensitivity, broad bandwidth, good galvanic insulation and noise immunity [15].

Recently, silicon-organic hybrid (SOH) technology [16] has shown to enable high performance integrated photonic devices such as compact and low-power EO modulators [17], [18], high-speed optical interconnects [19], [20], and sensitive photonic sensors [21]. Benefiting from the large EO coefficient (r_{33}) of active organic polymers [22], [23] as well as the strong optical mode confinement made possible by the large index of silicon [24], [25], SOH integrated photonic electromagnetic field sensors are promising for achieving high sensitivity, compact size, and broad bandwidth.

It has been demonstrated in [15] that low half-wave voltage (V_π), high input driving voltage (electric field), and large input optical power of EO modulators can improve the sensitivity of the photonic electromagnetic field sensors. To enhance the sensitivity through V_π reduction, silicon slot photonic crystal waveguides (PCWs) refilled with large EO coefficient (r_{33}) EO polymer can be employed due to the slow-light enhanced

light-matter interaction [26], [27]. The enhanced light-matter interaction also enables a compact device size [28], [29]. The silicon in the SOH slot PCW modulator can also be doped to achieve high speed operation [30], [31]. For example, modulation speeds up to 40 GHz or over 40 Gbit/s have been demonstrated in [32], [33]. Furthermore, the antenna can be designed for broadband resonant electric field enhancement (FE) [34], [35], which is equivalent to increasing the input driving voltage of the modulator, thereby increasing the sensitivity of the sensor. The geometrical dimensions of the antenna are much smaller than the wavelength of the electromagnetic field to be measured. This antenna can be combined with the SOH slot PCW modulator to achieve even higher sensitivity over wide frequency bandwidth. Such a combination of integrated RF photonics [36] and SOH technology [16] offers a viable platform for high frequency electromagnetic field sensing.

In this paper, we design and demonstrate an integrated photonic electromagnetic field sensor based on a bowtie antenna coupled SOH slot PCW modulator. The measured S-parameters show that the bowtie antenna with slot PCW embedded inside its feed gap has broadband characteristic, with a resonance peak at 10 GHz. High frequency electromagnetic field sensing is experimentally demonstrated through EO modulation at 8.4 GHz, with a minimum detectable electromagnetic power density of $8.4\,\mathrm{mW/m^2}$, corresponding to an incident electric field as small as 2.5 V/m. To the best of our knowledge, this is the first silicon-organic hybrid device used for the photonic sensing of electromagnetic fields.

II. DESIGN

A. Device Overview

The key parts of our photonic electromagnetic field sensor consisting of an EO polymer refilled silicon slot PCW phase modulator coupled with a gold bowtie-shaped antenna are shown schematically in Figs. 1(a)–(e). An EO polymer, SEO125 from Soluxra, LLC, with a large r_{33}, low optical loss, and good temporal stability, is used to refill the silicon slot PCW. This EO polymer refilled silicon slot PCW with a slot width (S_w) of 320 nm is band-engineered to achieve low-dispersion slow-light propagation over a broad wavelength range of 8 nm [37], as well as high optical mode confinement inside the EO polymer refilled slot. The slow-light enhanced effective in-device r_{33} of this SOH modulator can be over 1000 pm/V [18], [37], which is beneficial for high-sensitivity sensing. The slot PCW is embedded in the feed gap of the bowtie antenna, and the silicon layer is selectively implanted with different ion concentrations for high frequency operation [38]. The bowtie antenna is used as a receiving antenna, driving electrodes, and poling electrodes. Here the bowtie antenna with capacitive extension bars has a simple design, and a broadband characteristic. With the two bowtie arms as receivers, a confined resonant electric field with strong enhancement factor can be generated in the gap between them [34].

The working principle of this integrated photonic electromagnetic field sensor is discussed as follows. A continuous wave (CW) laser input is coupled into and out of the device.
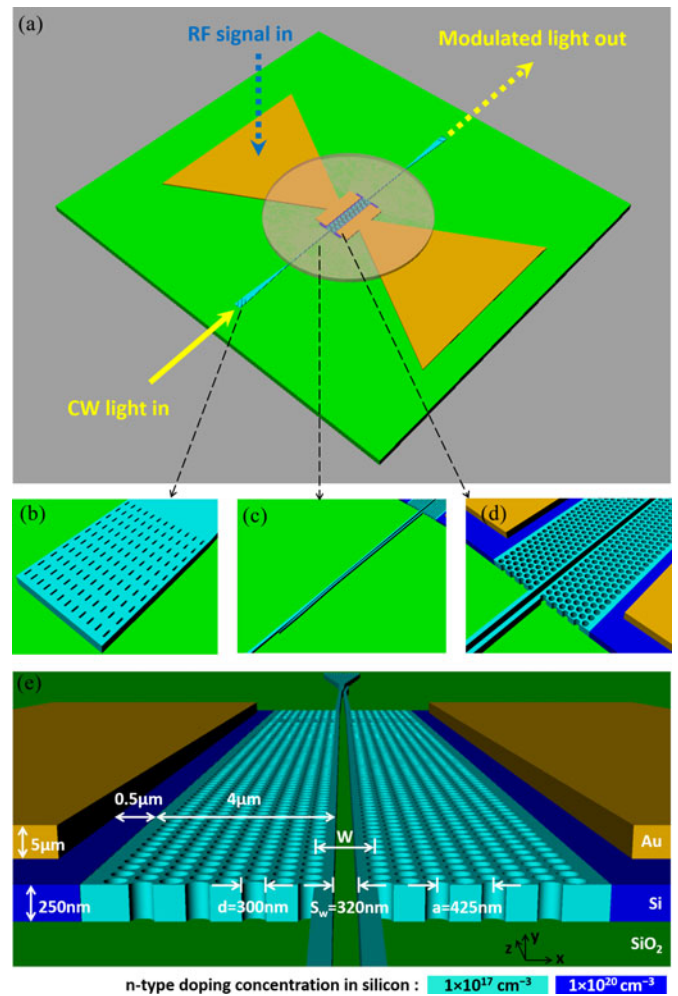

Fig. 1. (a) A schematic view of the key part of the electromagnetic field sensor consisting of an EO polymer refilled silicon slot PCW phase modulator and a bowtie antenna. An external arm combined with this phase modulator forms an MZI structure, converting phase modulation to intensity modulation. (b) SWG coupler. (c) Strip-to-slot mode converter. (d) Magnified image of slot PCW. (e) Tilted view showing the cross section of the antenna-coupled slot PCW, with dimension parameters and two levels of n-type silicon doping concentrations. Note: the EO polymer layer covered on top of the device is not shown in (b)–(e) for better visualization.

The bowtie antenna harvests incident electromagnetic waves, transforms it into high-power-density time-varying electric field within the feed gap, which directly interacts with the light propagating along the EO polymer refilled slot PCW embedded within the feed gap (i.e., interaction region). The refractive index of the EO polymer is controlled by the applied electric field via the EO effect, which modulates the phase of the optical wave within the low-dispersion wavelength regime of the slot PCW. For measurement, we convert this phase modulation to an intensity modulation using an external arm enabled MZI structure. Finally, by measuring the modulated optical intensity at the output end of the MZI, an incident electromagnetic field from free space can be detected through optical means. This integrated photonic electromagnetic field sensor can reduce the impact of perturbing fields, since it is based on an optical modulation technique.
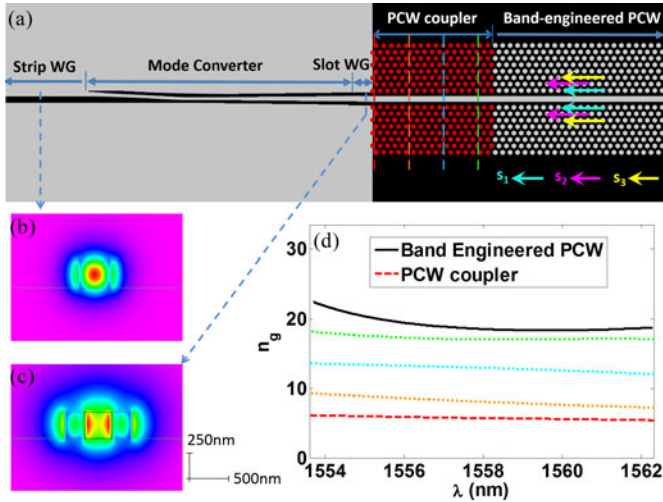
Fig. 2. (a) Layout of the strip-to-slot mode converter, PCW coupler and band-engineered PCW. The black area corresponds to unetched silicon, and the gray area corresponds to the etched silicon. The red-color holes indicate the PCW taper section. The s_1, s_2, and s_3 indicate the lattice shift direction in band-engineered PCW section. WG: waveguide. (b) Cross-sectional view of strip waveguide mode profile. (c) Cross-sectional view of slot waveguide mode profile. (d) The small variations of n_g over about 8-nm wavelength range, for the band-engineered slow-light PCW and PCW coupler. The lines of different colors represent the n_g at different positions along the PCW coupler as indicated by the dashed lines of corresponding colors in (a). This indicates a smooth transition of n_g from the beginning of the PCW taper to the band-engineered PCW.

B. Design of SOH Slot PCW Modulator

The layout of the slot PCW is shown in Fig. 2(a), including strip waveguide, mode converter, slot waveguide, PCW coupler and band-engineered PCW. This slot PCW is designed on a silicon-on-insulator (SOI) substrate with 250 nm-thick top silicon and 3 μm-thick buried oxide layers. The PCW holes and slot are assumed to be filled with EO polymer, SEO125, which has a refractive index of 1.63 at 1550 nm. SEO125 exhibits an exceptional combination of large EO coefficient, good near-infrared transparency, excellent chemical- and photo-stability, and improved processability [37]. Additionally, a lattice-shifted slot PCW is used to achieve low-dispersion slow light [39], where optimized values of the lattice constant ($a = 425$ nm), hole diameter ($d = 300$ nm), slot width ($S_w = 320$ nm), center-to-center distance between two rows adjacent to the slot ($W = 1.54(\sqrt{3})a$), relative lateral shift of the first three rows ($s_1 = 0, s_2 = -85$ nm, $s_3 = 85$ nm [indicated by the arrows in Fig. 2(a)]) are utilized. A group index (n_g) of 20.4 ($\pm 10\%$) over about 8 nm optical wavelength is achieved [37], as shown by Rsoft BandSolve simulations in Fig. 2(d), thereby enabling a relatively large operational optical bandwidth of sensor device compared to non-band-engineered PCW designs with typically narrow optical bandwidth of <1 nm at $n_g > 10$ [40]. Note that the large slot width of $S_w = 320$ nm in the PCW not only supports a confined optical mode, but also helps in increasing the poling efficiency by suppressing the leakage current in EO polymer poling process [37], [41]. In order to efficiently couple light between the slow-light mode of the slot PCW ($n_g \sim 20.4$) and the fast-light mode in the

slot waveguide at the mode converter end ($n_g \sim 3$), a PCW taper consisting of non-band-engineered PCW ($a = 425$ nm, $d = 300$ nm, $s_1 = 0, s_2 = 0, s_3 = 0, S_w = 320$ nm) is designed and inserted between the two device components, as indicated in Fig. 2(a), in which W increases parabolically from W = $1.45(\sqrt{3})$a to W = $1.54(\sqrt{3})$a from the beginning to the end of the PCW taper. Fig. 2(d) shows the n_g variation of the PCW taper over about 8 nm wavelength range for the engineered slow-light PCW and the PCW coupler. The colored dashed lines show the gradual increase in the group index from the interface with the mode converter to the interface with the high n_g band-engineered PCW. What is more, a new type of strip-to-slot mode converter that we have recently developed [42] is used to couple light between the strip waveguide and the 320 nm-wide-slot PCW waveguide more efficiently compared to conventional V-shape mode converters [43]. In addition, subwavelength grating (SWG) couplers [44], [45], as shown in Fig. 1(b), are used to couple light into and out of the device using single mode fibers.

The basic sensing principle is based on the EO modulation inside the EO polymer refilled silicon slot PCWs. The required PCW interaction length for achieving a π phase shift is given as $L = 1/(2\sigma) \times (n/\Delta n) \times \lambda/n_g = 255.9$ μm, where $\sigma = 0.33$ is the fraction of the energy in the slot calculated using Band-Solve simulations, $n = 1.63$ is the index of the EO polymer, $\Delta n = 0.0007$ is the change in the index of the EO polymer when voltage $V = 1$ V is applied, and $\lambda = 1550$ nm is the free-space wavelength and $n_g = 20.4$ is the group index. The change in the EO polymer index is calculated using $\Delta n = -n^3 r_{33} V/(2S_w)$, where the estimated $r_{33} = 100$ pm/V at 1550 nm is consistent with the large r_{33} value of 125 pm/V of SEO125 thin films at 1.3 μm after considering the dispersion factor and the nearly 100% poling efficiency demonstrated in 320 nm-wide slots [37]. Therefore, from these calculations, the figure of merit of the modulator is $V_\pi \times L = 1$ V $\times 255.9$ μm = 0.0256 V $\times$ cm. Such a small $V_\pi \times L$ promises a compact and efficient EO modulator, and thus a highly sensitive integrated photonic electromagnetic field sensor. The expected effective in-device r_{33} is then calculated as [46]

$$r_{33,\text{effective}} = \frac{\lambda S_w}{n^3 V_\pi \sigma L} = 1356 \, \text{pm/V}. \qquad (1)$$

Our another recent work has experimentally demonstrated the $V_\pi \times L$ and effective in-device r_{33} on the same order [37]. Conservatively, the length of the active section of the PCW used in our work is chosen to be 300 μm.

C. Design of RF Bowtie Antenna

To achieve modulation (or sensing) in GHz frequency regime, both the silicon PCW layer and the bowtie antenna need to be specially designed and carefully optimized. It is known that the RC time delay of a device is one key factor limiting its operational bandwidth. In order for our sensor to operate at a high frequency, the top silicon layer is doped to reduce the electrical resistivity of the PCW, while maximizing the electric field inside the slot. The designed two-level doping condition in the silicon slot PCW is shown in Fig. 1(e). The resistivity values of
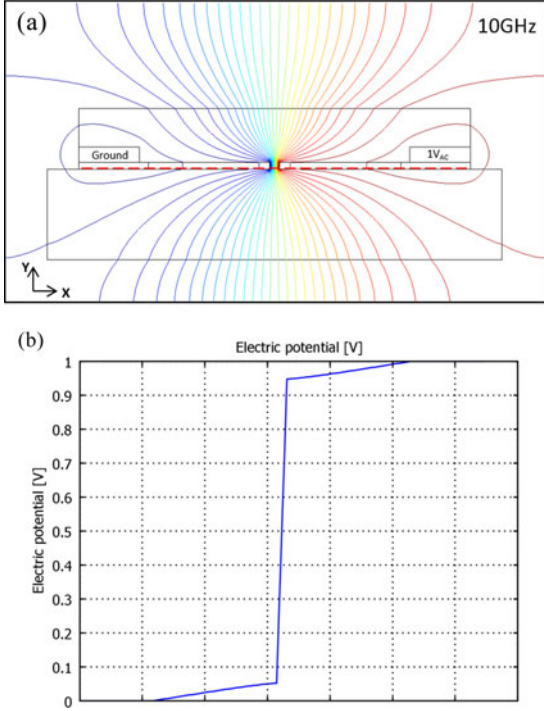
Fig. 3. (a) Cross-sectional view of RF (10 GHz) electric potential distribution across the doped silicon slot PCW filled with EO polymer. (b) Electric potential along the red dashed line in (a), indicating that a large percent of voltage is dropped across the slot filled with EO polymer.

Fig. 4. (a) Schematic top view of the designed bowtie antenna. Arm length, $L = 3$ mm, and flare angle, $\alpha = 60°$. (b) Magnified image of the feed gap region in (a). (c) Top view of electric field enhancement distribution inside the feed gap of the antenna. The electric field enhancement distribution is shown inside the EO polymer refilled slot at $y = 0.125 \ \mu$m, where $y = 0$ corresponds to the horizontal interface between the silicon layer and the buried oxide layer. (d) Variation of the field enhancement factor inside the slot versus incident RF frequency.

the highly-doped silicon (donor, 1×10^{20} cm^{-3}) and low-doped (donor, 1×10^{17} cm^{-3}) are $9 \times 10^{-6} \ \Omega \cdot$ m and $9 \times 10^{-4} \ \Omega \cdot$ m, respectively [47]. For reference, the intrinsic doping concentration of the undoped top silicon on our SOI wafer is 1×10^{14} cm^{-3}. Note that an ion doping concentration of 1×10^{17} cm^{-3} in the waveguide region close to optical mode does not cause significant impurity-induced scattering optical loss [48]. Based on our previous work [17], [41], [49], [50], in the case of 320 nm-wide slots, we use the EO polymer resistivity (ρ_{EO}) value of about $10^8 \ \Omega \cdot$ m and RF dielectric constant ($\varepsilon_{\mathrm{RF,EO}}$) value of 3.2. The change in the RF dielectric constant of silicon ($\varepsilon_{\mathrm{RF,Si}}$) due to the doping is also taken into account [51]. Then, effective medium approximations [52] are used for the calculation of both the effective RF dielectric constant ($\varepsilon_{\mathrm{RF,eff}}$) and the effective resistivity (ρ_{eff}) in the region of EO polymer refilled silicon PCW shown in Fig. 1(e) [hexagonal lattice, filling factor (volume fraction): $f = 0.444$]. The effective RF dielectric constant (electric field in x-direction) in this region is given as [53]

$$\varepsilon_{RF,\mathrm{eff}} = \varepsilon_{RF,Si} \left[\frac{\varepsilon_{RF,EO} \left(1 + f \right) + \varepsilon_{RF,Si} \left(1 - f \right)}{\varepsilon_{RF,EO} \left(1 - f \right) + \varepsilon_{RF,Si} \left(1 + f \right)} \right]. \quad (2)$$

The effective resistivity in this region is estimated as [54]

$$\rho_{\mathrm{eff}} = \rho_{Si} \left(\frac{1 + f}{1 - f} \right) \quad (3)$$

where, ρ_{si} is the resistivity of un-patterned silicon.

Fig. 3(a) shows the cross-sectional view of the RF electric potential distribution ($1V_{\mathrm{AC}}$, 10 GHz) across the doped silicon
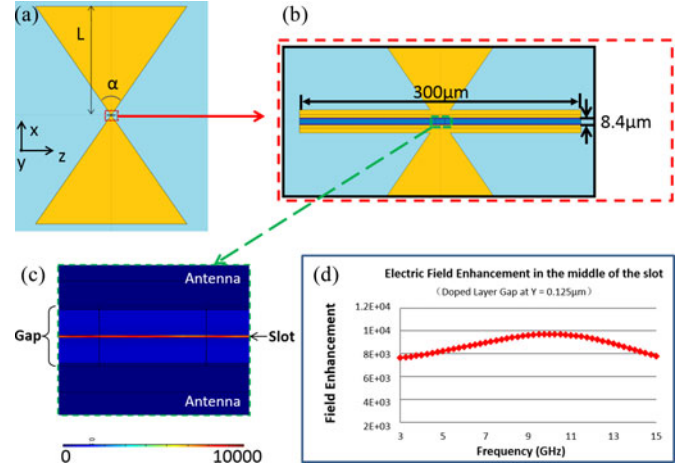
slot PCW, simulated by COMSOL MULTIPHYSICS, with the antenna replaced by perfect conductors. Fig. 3(b) shows that the voltage drop (>90%) mostly occurs inside the slot. As the RF frequency (f_{RF}) increases, the impedance of the slot ($1/(\mathrm{C}\omega)$), where C is slot capacitance and $\omega = 2\pi f_{\mathrm{RF}}$) decreases, and the fraction of the voltage dropped across the slot is reduced due to the finite resistance of the silicon PCW. For this two-level doping condition, a simulation using LUMERICAL DEVICE software shows that the total resistance of our 300 μm-long silicon PCW is 189 Ω and the slot capacitance is 38.6 fF, so the limiting RF frequency bandwidth of the device can be estimated to be $1/(2\pi RC) = 22$ GHz.

As shown in Figs. 4(a) and (b), the antenna is a conventional bowtie antenna with capacitive extension bars attached to the apex points of the bowtie, in order to obtain an extended area with a strong uniform electric FE. The extension bars have a length of 300 μm, which is the same as the length of EO polymer refilled slot PCW. The narrow feed gap width between the two capacitive bars is 8.4 μm, for the generation of highly enhanced local electric field under RF illumination. The thickness of the gold film is chosen to be 5 μm, which is far beyond the skin depth of gold at the RF frequency of operation. This gold antenna is designed with bow arms on silicon dioxide to avoid the impact of conductive silicon region. In the actual device fabricated on an SOI substrate, the top silicon region everywhere apart from the PCW region is entirely etched away, as shown in Fig. 5(b), letting the buried oxide layer be directly underneath the bow arms to fit this design. The silicon handle underneath the buried oxide layer is taken into account in the simulation.

Generally, the antenna system can be considered as a typical LC circuit, which is mainly composed of the inductive bowtie metallic arms and capacitive bars filled with EO polymer, giving rise to an LC resonance determined by antenna geometry [55]. In this work, this resonance effect is characterized by FE factor,
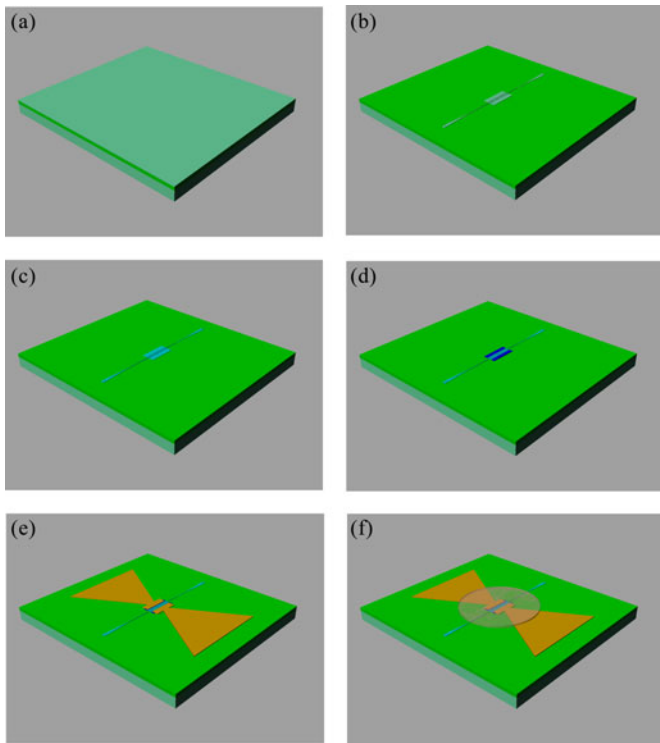
Fig. 5.   Fabrication flow. (a) SOI wafer, (b) Silicon photonic waveguide, patterned by electron-beam lithography, RIE, photolithography, and RIE again, (c) first ion implantation, (d) second ion implantation, followed by rapid thermal annealing (e) Gold bowtie antenna, patterned by seed layer deposition, photolithography, electroplating, and seed layer removal, (j) Spincoating of EO polymer (indicated by the circle area), followed by vacuum oven baking and EO polymer poling.

defined as the resonant electric field amplitude (inside the slot) divided by the incident electric field amplitude at the specific observation point. With the feed gap width and capacitive bars fixed, the resonant frequency of a bowtie antenna is mainly determined by the length of each bow arm and the flare angle [L and α in Fig. 4(a)] [56]. This bowtie antenna structure together with the effective-medium approximated silicon RF dielectric constant and conductivity values is used for COMSOL MULTIPHYSICS simulation. With bow arm length L = 3 mm and flare angle $\alpha = 60°$, the bowtie antenna is optimized with a central resonant frequency at around 10 GHz, and a uniform electric field enhancement over the entire feed gap is created. Fig. 4(c) show the top view of the local resonant electric field amplitude inside the antenna feed gap at 10 GHz. The electric field is mainly confined in the feed gap region, which is similar to the performance of a typical dipole antenna [57]. Additionally, as explained above, the electric field is actually concentrated inside the slot of the silcon PCW, and this increases the FE even further. Fig. 4(d) shows the FE spectrum from simulations, indicating that the electric field radiation compressed inside the slot of the silicon PCW is enhanced by a maximum factor of ∼10,000 at 10 GHz, with a 1-dB RF bandwidth over 9 GHz. This strongly enhanced RF field directly modulates the optical wave propagating along the EO polymer refilled doped silicon slot PCW which is embedded inside the feed gap. No extra connection lines between the antenna and EO modulator and no external electrical power supply are required [11]. Furthermore, similar

to a typical dipole antenna, the bowtie antenna has spatially wide angular beamwidth in its radiation pattern, which enables our sensor to detect electromagnetic fields from a large range of incident angles.

III. FABRICATION

The fabrication flow is briefly illustrated in Fig. 5. The fabrication starts with an SOI wafer with a 250 nm-thick top silicon and a 3 μm-thick buried oxide layer, as shown in Fig. 5(a). The silicon slot PCW is fabricated using electron-beam lithography and reactive ion etching (RIE). Next, all of the top silicon region, except the area with the slot PCW, is completely removed by photolithography and RIE, as shown in Fig. 5(b). Then, the silicon slot PCW is first implanted with P+ at an energy of 92 keV and a dose of 1.05×10^{12} cm^{-2} to reach an ion concentration of 1×10^{17} cm^{-3} [see Fig. 5(c)]. Next, the device is patterned by photolithography and implanted with P+ at an energy of 92 keV and a dose of 1.05×10^{15} cm^{-2} to reach an ion concentration of 1×10^{20} cm^{-3} at the outer sides of the silicon rails which will be connected to the bowtie antenna in order to form Ohmic contacts [see Fig. 5(d)]. A rapid thermal annealing at 1000 °C for 10 sec in a nitrogen environment is then performed to annihilate the induced defects and to activate the implanted ions, which also improves the optical performance of the ion-implanted waveguides [58]. Next, a 50 nm-thick gold seed layer with a 5 nm-thick chromium adhesion buffer is deposited by electron-beam evaporation, and a buffer mask for the bowtie antenna is patterned on a 10 μm-thick AZ9260 photoresist using photolithography. Then, a 5 μm-thick gold film is electroplated using Techni-Gold 25ES electrolyte under a constant current of 8 mA. The AZ9260 buffer mask and gold seed layer are finally removed by lift-off and wet etching, as shown in Fig. 5(e). SEM images of the fabricated device are shown in Fig. 6. The inner sides of the extension bars of the bowtie antenna are connected to the outer sides of silicon rails which are heavily doped for Ohmic contact between the antenna and the PCW, as shown in Fig. 6(b).

Next, the EO polymer, SEO125, is formulated and infiltrated into the holes and the slot of the silicon PCW region by spincoating, as shown in Fig. 5(f), followed by baking at 80 °C in vacuum oven for 12 h. To align the polymer chromophore noncentrosymmetrically, the EO polymer is poled at a constant electric field of 110 V/μm at the EO polymer glass transition temperature of 145 °C, in which the bowtie antenna serves as poling electrodes. During this poling process, the monitored leakage current density remains below 8.8 A/m^2 which is comparable to that measured in a thin film configuration (1 – 10 A/m^2) [37], indicating that the 320 nm-wide slot dramatically reduces the leakage current through the silicon/polymer interface compared to sub-100 nm slot designs [37], [41].

IV. CHARACTERIZATION

A. Bowtie Antenna Characterization

In order to demonstrate the broadband characteristics of the fabricated bowtie antenna, a network analyzer (HP 8510C) is
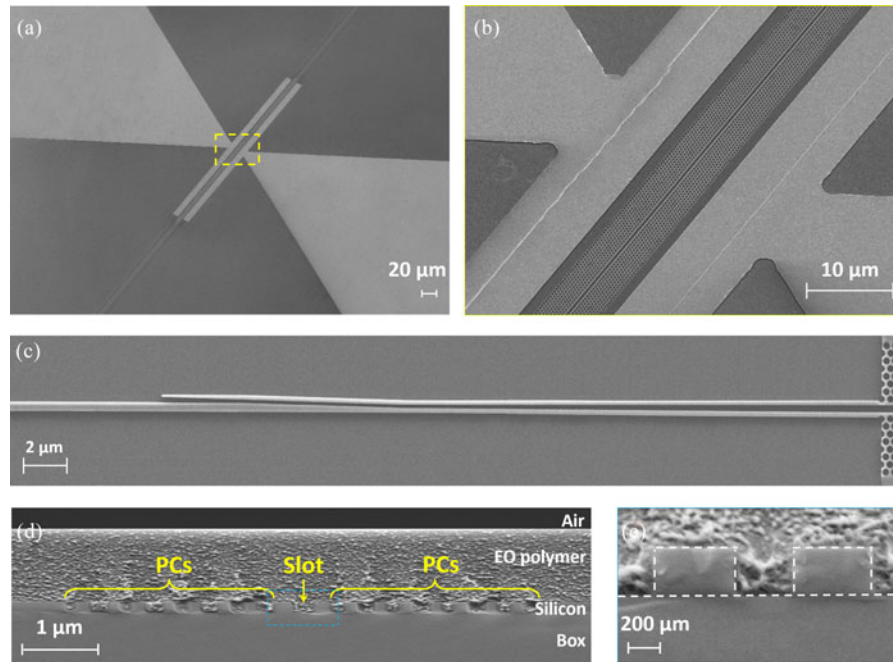
Fig. 6. (a) SEM image of the fabricated device. (b) Magnified SEM image of the yellow rectangular region in (a) showing the slot PCW region and bowtie antenna overlay. (c) SEM image of the strip-to-slot mode converter for efficient coupling between strip waveguide and the 320 nm slot PCW. Note: in (a)–(c) the device is not covered by EO polymer, just for better visualization. (d) SEM image of the cross section of the EO polymer refilled silicon slot PCW. PCs: photonic crystals. (e) Magnified SEM image of the blue rectangular area in (d).
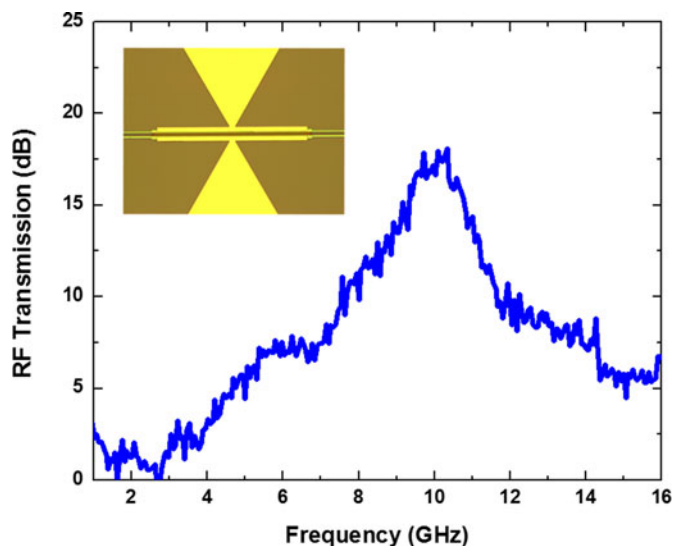

Fig. 7. Measured transmission signal of the broadband bowtie antenna. The inset shows a top-view microscope image of the fabricated device.

used to measure the S_{11} parameter (reflection coefficient) of the bowtie antenna. A ground-signal (GS) microprobe (Cascade Microtech ACP40GS500) is used to couple RF power from the network analyzer into the bowtie antenna, and the S_{11} parameter over a broad frequency range from 1–16 GHz is recorded. Assuming negligible loss, the transmission factor can be inferred from the S_{11} measurements, as shown in Fig. 7, from which a broadband response can be clearly seen. The maximum response occurs at 10 GHz, which agrees well with the simulated

maximum field enhancement at 10 GHz in Fig. 4(d). Considering the reciprocity of the bowtie antenna, this result indicates that our sensor can be used to receive the electromagnetic field over a broad frequency bandwidth in the GHz regime.

B. Optical Waveguide Characterization

In order to test the EO polymer refilled silicon slot PCW, light from a broadband amplified spontaneous emission (ASE) source (Thorlabs ASE730) is coupled into and out of the device utilizing an in-house built grating coupler setup [44], [45]. The optical output signal is observed on an optical spectrum analyzer (OSA, Ando AQ6317B). Fig. 8 shows the measured normalized transmission spectrum of the EO polymer refilled silicon slot PCW. A clear band gap with more than 25 dB contrast is observed, indicating efficient coupling into the slot PCW.

C. Electro-Optic Modulation Experiment

With the RF path and optical path separately verified, as explained in Sections IV-A and IV-B, an EO modulation experiment is then performed. An MZI system is formed, using a 90/10 polarization maintaining fiber splitter (Thorlabs L130354603), a 50/50 polarization maintaining fiber combiner (Thorlabs L110313487) and a variable optical attenuator (VOA, Thorlabs VOA50PM-FC), as shown in Fig. 9. A low-frequency modulation test is performed here to verify the functionality of this MZI system.

A tunable laser source (Santec ECL200) is used to provide TE-polarized optical input. The optical wavelength is tuned to 1556 nm which is within the low-dispersion region of the
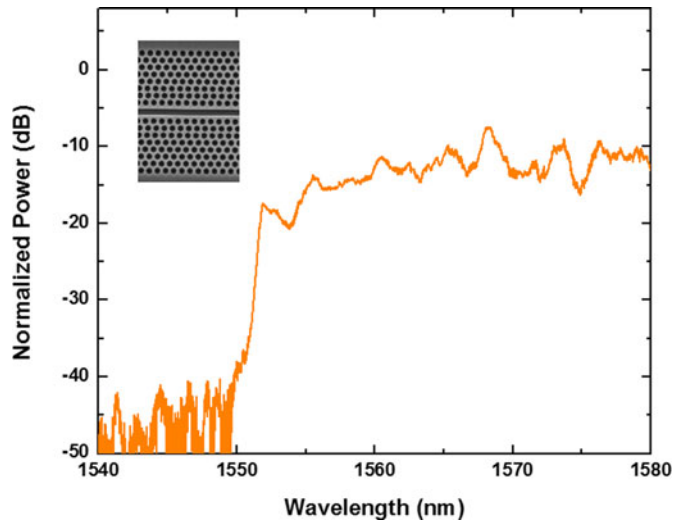
Fig. 8.   Normalized transmission spectrum of the EO polymer refilled silicon slot PCW. The inset shows an SEM image of the fabricated silicon slot PCW.
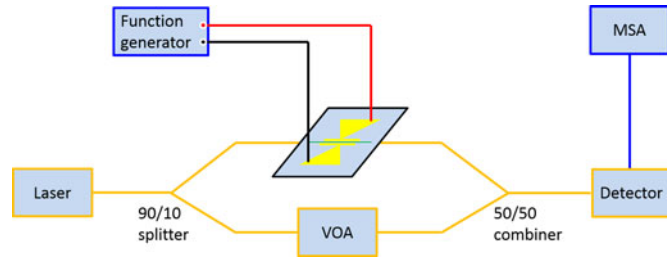

Fig. 9.   The schematic of the system for EO modulation experiment. VOA: variable optical attenuator. MSA: microwave spectrum analyzer.

band-engineered PCW. The laser input is split by a 90/10 splitter, in which 90% of the optical power is coupled into and out of the sensor device through SWG couplers and 10% goes to the external arm with the VOA. Next, the VOA is adjusted until the optical power at the output of the external arm is equal to that coming out of the sensor device. A 50/50 combiner is then used to combine the optical waves from the two arms, so that the phase modulation can be converted into intensity modulation at the output of this MZI system. A sinusoidal RF signal with a peak-to-peak voltage (V_{pp}) of 1 V at a frequency of 100 KHz is generated using a function generator (Agilent 33120A) and directly applied across the two arms of the bowtie antenna. In this case, the two arms work as lumped-element driving electrodes and directly modulate the optical waves propagating in the slot PCW embedded in the feed gap of the bowtie antenna. The modulated output optical signal is converted back to an electrical signal using an amplified photodetector (Thorlabs PDA10CS), whose power is measured on a microwave spectrum analyzer (MSA, HP 8563E), as shown in Fig. 10(a). The measured response signal in Fig. 10(a) indicates that the optical signal is modulated at the same frequency as the input RF signal. When the laser is switched off, this response signal on the MSA disappears, confirming that the signal measured by the MSA originates from the real EO modulation instead of RF cross talk. The EO modulation experiment also demonstrates
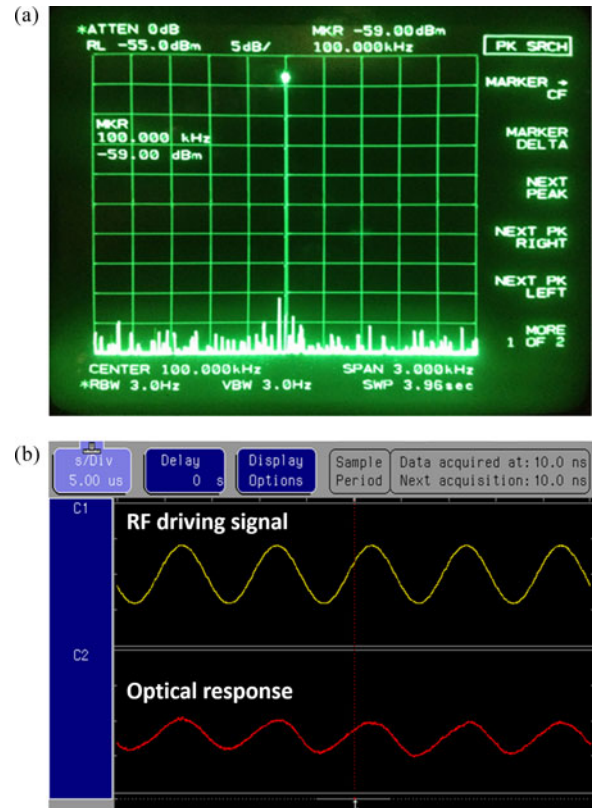

Fig. 10.   (a) The EO modulation response signal as measured on the MSA. (b) EO modulation transfer function.
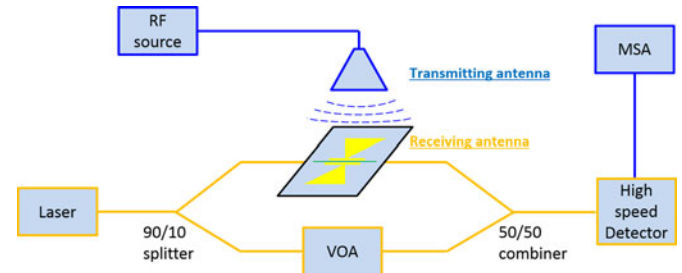

Fig. 11.   The schematic of the system setup for electromagnetic field sensing experiment. VOA: variable optical attenuator. MSA: microwave spectrum analyzer.

the successful poling of the EO polymer and the functionality of the MZI system, which is then used in the sensing experiment in Section IV-D.

Another small signal modulation test further demonstrates the validity of the EO modulation, in which an integrated MZI modulator device is fabricated on a chip, with the same EO polymer refilled PCW on both arms [37]. The modulator is driven by a sinusoidal RF signal with $V_{pp} < 1V$ at 100 KHz. The modulation transfer function is measured by a logic analyzer (HP 1660ES) and shown in Fig. 10(b).

D. Electromagnetic Field Sensing Experiment

The schematic of the experimental system setup for the electromagnetic field sensing is shown in Fig. 11. A sweep oscillator (8620C HP, 2–8.4 GHz) is used as a high-frequency RF source
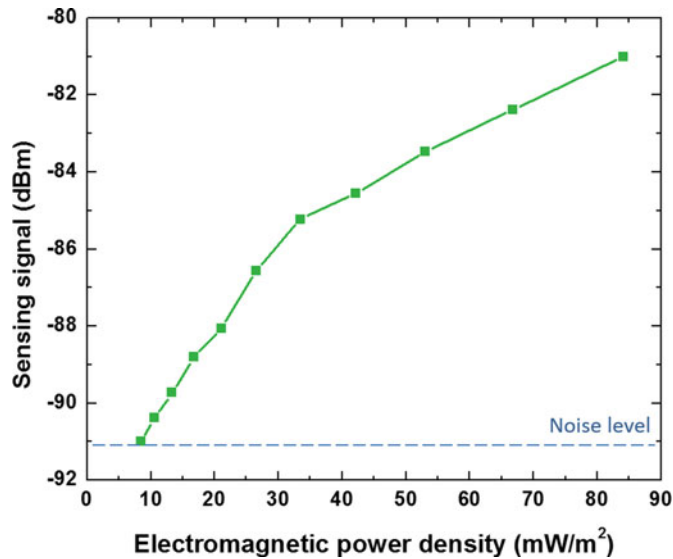
Fig. 12. The measured sensing signal at 8.4 GHz as a function of the electromagnetic power density at the position of sensor device.

to provide an RF signal at a frequency of 8.4 GHz. This RF signal is applied to an X-band horn antenna with a gain of 6 dB. In this case, the horn antenna works as a transmitting antenna to generate electromagnetic field in free space, and the bowtie antenna in our device works as a receiving antenna to detect the electromagnetic field impinging upon it. The horn antenna is placed at a distance of 30 cm vertically over the sensor device, which is beyond the far-field distance of the horn antenna so that the electromagnetic waves radiating on the sensor can be treated as plane waves in the following experimental data analysis. To detect the modulated optical signal at high frequency, a high-speed photodetector (Discovery Semiconductors, DSC40S) is used, and the sensing signal is measured on the MSA.

To characterize the sensitivity of this sensor in terms of electromagnetic power density (or electric field magnitude), the RF power applied on the horn antenna is varied. The corresponding variation in the electromagnetic power density radiating to the position of sensor device is calculated based on Eq. (4) [59]

$$S_{\text{avg}} = \frac{G_t P_t}{4\pi R^2} \quad (4)$$

where S_{avg} is the average Poynting vector (electromagnetic power density, unit: mW/m^2), $G_t = 6$ dB is the gain of the transmitting horn antenna, P_t is the input RF power applied on the horn antenna, $R = 30$ cm is the distance between the horn antenna and the sensor device. The measured sensing signal as a function of electromagnetic power density is plotted in Fig. 12. It can be seen that the sensing signal decreases as the electromagnetic power density decreases. When the electromagnetic power density decreases to 8.4 mW/m^2 (equivalent to the input RF power of 2 dBm applied on the horn antenna) at 8.4 GHz, the sensing signal is below the noise level. Based on Eq. (5), this minimum detectable electromagnetic power density (8.4 mW/m^2) is used to estimate the minimum detectable electric field amplitude ($|E|$) as 2.5 V/m at 8.4 GHz, considering the electromagnetic field has a predominantly plane-wave character

within the far-field region of the horn antenna [60]

$$|E| = \sqrt{\frac{2S_{\text{avg}}}{\varepsilon_0 \varepsilon_r c}} = 2.5 \text{V/m} \quad (5)$$

where $\varepsilon_0 = 8.85 \times 10^{-12}$ F/m is the vacuum dielectric constant, $\varepsilon_r \approx 1$ is the dielectric constant of air, $c = 3 \times 10^8$ m/s is the speed of light. Given the FE, for this incident field, the electric field inside the slot is about 2.5×10^4 V/m. In addition, the measurement of the maximum detectable electric field is limited by the upper limit of the output power of the RF source. In practice, the maximum detectable electric field is expected to be very high and is determined by the breakdown electric field of the EO polymer material ($>1 \times 10^8$ V/m).

As for the electromagnetic field frequency, our sensor has the potential to detect the electromagnetic field over a broad bandwidth, because the bowtie antenna has been demonstrated for broadband operation in GHz frequency regime in Section IV-A. Our sensor is also promising for low-frequency electromagnetic field sensing, because an EO activity with ultrahigh r_{33} of 1190 pm/V at a low modulation frequency of 100 kHz has been demonstrated using the same EO polymer refilled slot PCW in our another recent work [37].

V. Conclusion

We design, fabricate and experimentally demonstrate a compact and sensitive integrated photonic electromagnetic field sensor based on EO polymer refilled silicon slot PCW coupled with a miniaturized bowtie antenna. The bowtie antenna is used as receiving antenna, poling electrodes and driving electrodes. The bowtie antenna with doped silicon slot PCW embedded inside its feed gap is demonstrated to have broadband characteristics with a maximum response at 10 GHz. Slow-light effects in the PCW, large EO coefficient polymer, as well as broadband electric field enhancement provided by the bowtie antenna, are all utilized to enhance the EO modulation efficiency, leading to a very high sensitivity. The minimum detectable electromagnetic power density is demonstrated to be 8.4 mW/m^2 at 8.4 GHz, corresponding to the minimum electric field amplitude of 2.5 V/m.

References

[1] P. Drexler and P. Fiala, "Methods for high-power EM pulse measurement," *IEEE Sens. J.*, vol. 7, no. 7, pp. 1006–1011, Jul. 2007.
[2] Q. Wu and X. C. Zhang, "Ultrafast electro-optic field sensors," *Appl. Phys. Lett.*, vol. 68, pp. 1604–1606, 1996.
[3] H. Bassen and G. Smith, "Electric field probes–A review," *IEEE Trans. Antennas Propag.*, vol. AP-31, no. 5, pp. 710–718, Sep. 1983.
[4] A. Pedersen, C. Cattell, C.-G. Fälthammar, V. Formisano, P.-A. Lindqvist, F. Mozer, and R. Torbert, "Quasistatic electric field measurements with spherical double probes on the GEOS and ISEE satellites," *Space Sci. Rev.*, vol. 37, pp. 269–312, 1984.

[5] G. Gustafsson, R. Boström, B. Holback, G. Holmgren, A. Lundgren, K. Stasiewicz, L. Åhlén, F. Mozer, D. Pankow, and P. Harvey, "The electric field and wave experiment for the Cluster mission," in *The Cluster and Phoenix Missions*. New York, NY, USA: Springer, 1997, pp. 137–156.

[6] H. Bassen, C. Bulmer, and W. Burns, "An RF field strength measurement system using unintegrated optical linear modulator," in *Proc. IEEE MTT-S Int. Microw. Symp. Dig.*, 1980, pp. 317–318.

[7] N. A. Jaeger and L. Young, "High-voltage sensor employing an integrated optics Mach-Zehnder interferometer in conjunction with a capacitive divider," *J. Lightw. Technol.*, vol. 7, pp. 229–235, 1989.

[8] W. B. Bridges, F. T. Sheehy, and J. H. Schaffner, "Wave-coupled LiNbO/sub 3/electrooptic modulator for microwave and millimeter-wave modulation," *IEEE Photon. Technol. Lett.*, vol. 3, no. 2, pp. 133–135, Feb. 1991.

[9] F. T. Sheehy, W. B. Bridges, and J. H. Schaffner, "60 GHz and 94 GHz antenna-coupled LiNbO3 electrooptic modulators," *IEEE Photon. Technol. Lett.*, vol. 5, no. 3, pp. 307–310, Mar. 1993.

[10] Y. Wijayanto, H. Murata, and Y. Okamura, "Electro-optic wireless millimeter-wave-lightwave signal converters using planar Yagi-Uda array antennas coupled to resonant electrodes," in *Proc. 17th Opto-Electron. Commun. Conf.*, 2012, pp. 543–544.

[11] Y. N. Wijayanto, H. Murata, and Y. Okamura, "Electrooptic millimeter-wave–lightwave signal converters suspended to gap-embedded patch antennas on low-dielectric materials," *IEEE J. Select. Topics Quantum Electron.*, vol. 19, no. 6, p. 3400709, Nov./Dec. 2013.

[12] A. B. Matsko, A. A. Savchenkov, V. S. Ilchenko, D. Seidel, and L. Maleki, "On the sensitivity of all-dielectric microwave photonic receivers," *J. Lightw. Technol.*, vol. 28, pp. 3427–3438, 2010.

[13] N. Kuwabara, K. Tajima, R. Kobayashi, and F. Amemiya, "Development and analysis of electric field sensor using LiNbO₃ optical modulator," *IEEE Trans. Electromagn. Compat.*, vol. 34, no. 4, pp. 391–396, Nov. 1992.

[14] K. Tajima, R. Kobayashi, N. Kuwabara, and M. Tokuda, "Development of optical isotropic E-field sensor operating more than 10 GHz using mach-zehnder interferometers," *IEICE Trans. Electron.*, vol. 85, pp. 961–968, 2002.

[15] V. Passaro, F. Dell'Olio, and F. De Leonardis, "Electromagnetic field photonic sensors," *Progress Quantum Electron.*, vol. 30, pp. 45–73, 2006.

[16] J. Leuthold, W. Freude, J.-M. Brosi, R. Baets, P. Dumon, I. Biaggio, M. L. Scimeca, F. Diederich, B. Frank, and C. Koos, "Silicon organic hybrid technology—A platform for practical nonlinear optics," *Proc. IEEE*, vol. 97, no. 7, pp. 1304–1316, Jul. 2009.

[17] X. Zhang, B. Lee, C.-y. Lin, A. X. Wang, A. Hosseini, and R. T. Chen, "Highly linear broadband optical modulator based on electro-optic polymer," *IEEE Photon. J.*, vol. 4, no. 6, pp. 2214–2228, Dec. 2012.

[18] X. Zhang, A. Hosseini, C.-y. Lin, J. Luo, A. K. Jen, and R. T. Chen, "Demonstration of effective in-device r33 over 1000 pmV in electro-optic polymer refilled silicon slot photonic crystal waveguide modulator," presented at the CLEO: Sci. Innovations, San Jose, CA, USA, 2013, P. CTu2F. 6.

[19] F. E. Doany, C. L. Schow, B. G. Lee, R. Budd, C. Baks, R. Dangel, R. John, F. Libsch, J. A. Kash, and B. Chan, "Terabit/sec-class board-level optical interconnects through polymer waveguides using 24-channel bidirectional transceiver modules," in *Proc. IEEE 61st Electron. Components Technol. Conf.*, 2011, pp. 790–797.

[20] X. Zhang, A. Hosseini, X. Lin, H. Subbaraman, and R. T. Chen, "Polymer-based hybrid integrated photonic devices for silicon on-chip modulation and board-level optical interconnects," *IEEE J. Select. Topics Quantum Electron.*, vol. 19, no. 6, pp. 196–210, Nov./Dec. 2013.

[21] C.-Y. Lin, A. X. Wang, B. S. Lee, X. Zhang, and R. T. Chen, "High dynamic range electric field sensor for electromagnetic pulse detection," *Opt. Exp.*, vol. 19, pp. 17372–17377, 2011.

[22] L. Jingdong and A. K. Y. Jen, "Highly efficient organic electrooptic materials and their hybrid systems for advanced photonic devices," *IEEE J. Select. Topics Quantum Electron.*, vol. 19, no. 6, pp. 42–53, Nov./Dec. 2013.

[23] T.-D. Kim, J. Luo, Y.-J. Cheng, Z. Shi, S. Hau, S.-H. Jang, X.-H. Zhou, Y. Tian, B. Polishak, S. Huang, Ma. Hong, L. R. Dalton, and A. K.-Y. Jen, "Binary chromophore systems in nonlinear optical dendrimers and polymers for large electrooptic activities†," *J. Phys. Chemistry C*, vol. 112, pp. 8091–8098, 2008.

[24] R. Soref, "The past, present, and future of silicon photonics," *IEEE J. Select. Topics Quantum Electron.*, vol. 12, no. 6, pp. 1678–1687, Nov./Dec. 2006.

[25] B. Jalali and S. Fathpour, "Silicon photonics," *J. Lightw. Technol.*, vol. 24, pp. 4600–4615, 2006.

[26] T. Baba, "Slow light in photonic crystals," *Nature Photon.*, vol. 2, pp. 465–473, 2008.

[27] Y. A. Vlasov, M. O'Boyle, H. F. Hamann, and S. J. McNab, "Active control of slow light on a chip with photonic crystal waveguides," *Nature*, vol. 438, pp. 65–69, 2005.

[28] X. Zhang, A. Hosseini, J. Luo, A. K.-Y. Jen, and R. T. Chen, "Hybrid silicon-electro-optic-polymer integrated high-performance optical modulator," *Proc. SPIE OPTO*, vol. 8991, pp. 89910O-1–89910O-6, 2014.

[29] Y. Jiang, W. Jiang, L. Gu, X. Chen, and R. T. Chen, "80-micron interaction length silicon photonic crystal waveguide modulator," *Appl. Phys. Lett.*, vol. 87, p. 221105, 2005.

[30] X. Zhang, A. Hosseini, H. Subbaraman, S. Wang, Q. Zhan, J. Luo, A. Jen, and R. Chen, "Wideband electromagnetic wave sensing using electro-optic polymer infiltrated silicon slot photonic crystal waveguide," presented at the *CLEO: Sci. Innovations*, San Jose, 2014.

[31] X. Zhang, A. Hosseini, H. Subbaraman, J. Luo, A. K.-Y. Jen, R. L. Nelson, and R. T. Chen, "Broadband Low-power Optical Modulator Based on Electro-optic Polymer Infiltrated Silicon Slot Photonic Crystal Waveguide," in *Proc. Frontiers in Opt./Laser Sci. Conf.*, 2014, Paper FTu1D.4.

[32] J. H. Wülbern, S. Prorok, J. Hampe, A. Petrov, M. Eich, J. Luo, A. K.-Y. Jen, M. Jenett, and A. Jacob, "40 GHz electro-optic modulation in hybrid silicon–organic slotted photonic crystal waveguides," *Opt. Lett.*, vol. 35, pp. 2753–2755, 2010.

[33] L. Alloatti, D. Korn, R. Palmer, D. Hillerkuss, J. Li, A. Barklund, R. Dinu, J. Wieland, M. Fournier, and J. Fedeli, "42.7 Gbit/s electro-optic modulator in silicon technology," *Opt. Exp.*, vol. 19, pp. 11841–11851, 2011.

[34] S. Wang and Q. Zhan, "Modified bow-tie antenna with strong broadband field enhancement for RF photonic applications," *Proc. SPIE NanoSci. Eng.*, vol. 8806, pp. 88061V-1–88061V-6, 2013.

[35] X. Zhang, S. Wang, H. Subbaraman, A. Hosseini, Q. Zhan, and R. Chen, "Integrated Broadband Bowtie Antenna on Transparent Substrate," Presented in Photonic West Conference, SPIE, 2015, Paper No. OE106-10 (Submitted for publication).

[36] D. Marpaung, C. Roeloffzen, R. Heideman, A. Leinse, S. Sales, and J. Capmany, "Integrated microwave photonics," *Laser Photon. Rev.*, vol. 7, pp. 506–538, 2013.

[37] X. Zhang, A. Hosseini, S. Chakravarty, J. Luo, A. K. Y. Jen, and R. T. Chen, "Wide optical spectrum range, subvolt, compact modulator based on an electro-optic polymer refilled silicon slot photonic crystal waveguide," *Opt. Lett.*, vol. 38, pp. 4931–4934, 2013.

[38] X. Zhang, A. Hosseini, X. Xu, S. Wang, Q. Zhan, Y. Zou, S. Chakravarty, and R. T. Chen, "Electric field sensor based on electro-optic polymer refilled silicon slot photonic crystal waveguide coupled with bowtie antenna," in *Proc. SPIE OPTO*, vol. 8624, pp. 862418-1–862418-8, 2013.

[39] A. Hosseini, X. Xu, H. Subbaraman, C.-Y. Lin, S. Rahimi, and R. T. Chen, "Large optical spectral range dispersion engineered silicon-based photonic crystal waveguide modulator," *Opt. Exp.*, vol. 20, pp. 12318–12325, 2012.

[40] H. C. Nguyen, Y. Sakai, M. Shinkawa, N. Ishikura, and T. Baba, " 10 Gb/s operation of photonic crystal silicon optical modulators," *Opt. Exp.*, vol. 19, pp. 13000–13007, 2011.

[41] X. Wang, C.-Y. Lin, S. Chakravarty, J. Luo, A. K.-Y. Jen, and R. T. Chen, "Effective in-device r33 of 735 pm/V on electro-optic polymer infiltrated silicon photonic crystal slot waveguides," *Opt. Lett.*, vol. 36, pp. 882–884, 2011.

[42] X. Zhang, H. Subbaraman, A. Hosseini, and R. T. Chen, "Highly efficient mode converter for coupling light into wide slot photonic crystal waveguide," *Opt. Exp.*, vol. 22, no. 17, pp. 20678–20690, 2014.

[43] Z. Wang, N. Zhu, Y. Tang, L. Wosinski, D. Dai, and S. He, "Ultracompact low-loss coupler between strip and slot waveguides," *Opt. Lett.*, vol. 34, pp. 1498–1500, 2009.

[44] X. Xu, H. Subbaraman, J. Covey, D. Kwong, A. Hosseini, and R. T. Chen, "Complementary metal–oxide–semiconductor compatible high efficiency subwavelength grating couplers for silicon integrated photonics," *Appl. Phys. Lett.*, vol. 101, pp. 031109-1–031109-4, 2012.

[45] H. Subbaraman, X. Xu, J. Covey, and R. T. Chen, "Efficient light coupling into in-plane semiconductor nanomembrane photonic devices utilizing a sub-wavelength grating coupler," *Opt. Exp.*, vol. 20, pp. 20659–20665, 2012.

[46] A. Yariv and P. Yeh, *Optical Waves in Crystal Propagation and Control of Laser Radiation*. Hoboken, NJ, USA: Wiley, 1983.

[47] S. K. Ghandhi, *VLSI Fabrication Principles: Silicon and Gallium Arsenide*. Hoboken, NJ, USA: Wiley, 2008.

[48] J. Doylend, P. Jessop, and A. Knights, "Optical attenuation in ion-implanted silicon waveguide racetrack resonators," *Opt. Exp.*, vol. 19, no. 16, pp. 14913–14918, 2011.

[49] X. Lin, T. Ling, H. Subbaraman, X. Zhang, K. Byun, L. J. Guo, and R. T. Chen, "Ultraviolet imprinting and aligned ink-jet printing for multi-layer patterning of electro-optic polymer modulators," *Opt. Lett.*, vol. 38, pp. 1597–1599, 2013.

[50] H. Subbaraman, X. Lin, T. Ling, X. Zhang, L. J. Guo, and R. T. Chen, "Printable EO polymer modulators," presented at the CLEO: Science and Innovations, San Jose, CA, USA, 2013, P. CW1O. 2.

[51] S. Ristić, A. Prijić, and Z. Prijić, "Dependence of static dielectric constant of silicon on resistivity at room temperature," *Serbian J. Electr. Eng.*, vol. 1, pp. 237–247, 2004.

[52] T. C. Choy, *Effective Medium Theory: Principles and Applications*. London, U.K.: Oxford Univ. Press, 1999.

[53] D. Gao and Z. Zhou, "Nonlinear equation method for band structure calculations of photonic crystal slabs," *Appl. Phys. Lett.*, vol. 88, p. 163105, 2006.

[54] W. Perrins, D. McKenzie, and R. McPhedran, "Transport properties of regular arrays of cylinders," *Proc. Roy. Soc. London. A. Math. Phys. Sci.*, vol. 369, pp. 207–225, 1979.

[55] C. A. Balanis, *Antenna Theory: Analysis and Design*. Hoboken, NJ, USA: Wiley, 2012.

[56] J. D. Kraus and R. J. Marhefka, *Antenna for all Applications*, 3rd ed. New York: McGraw-Hill, 2002.

[57] H. Duan, A. I. Fernández-Domínguez, M. Bosman, S. A. Maier, and J. K. Yang, "Nanoplasmonics: Classical down to the nanometer scale," *Nano Lett.*, vol. 12, pp. 1683–1689, 2012.

[58] O. Peña-Rodríguez, J. Olivares, M. Carrascosa, Á. García-Cabañes, A. Rivera, and F. Agulló-López, "Optical waveguides fabricated by ion implantation/irradiation: A review," in *Ion Implantation*, M. Goorsky, Ed., In Tech, 2012, pp. 978–953.

[59] D. M. Pozar, *Microwave Engineering*, 4th ed. Hoboken, NJ: Wiley, 2011.

[60] A. Chen and E. J. Murphy, *Broadband Optical Modulators: Science, Technology, and Applications*. Boca Raton, FL, USA: CRC Press, 2011.

Xingyu Zhang (S'13) received the B.S. degree in electrical engineering from Beijing Institute of Technology, Beijing, China, in 2009, and the M.S. degree in electrical engineering from University of Michigan, Ann Arbor, MI, USA in 2010. He is currently working toward the Ph.D degree at the University of Texas, Austin, TX, USA.

His current research focuses on the design, fabrication, and characterization of silicon and polymer hybrid integrated microwave nanophotonic devices used in optical interconnects and RF sensing, including highly linear broadband optical modulators, high-speed sub-volt low-dispersion slot photonic crystal waveguide modulators, sensitive integrated photonic electromagnetic field sensors, highly efficient strip-to-slot mode converters, and broadband integrated antennas. He has published as the first author about 20 peer-reviewed papers in journals and conferences during the Ph.D. degree, including one invited paper in IEEE JOURNAL OF SELECTED TOPICS IN QUANTUM ELECTRONICS.

Mr. Zhang has so far served as reviewers for 13 prestigious journals in his research area. He is the recipient of Engineering Scholarship Award at UT-Austin and Full Financial Fellowship at UM-Ann Arbor. He has industry internship experiences in IBM and Oracle. He is a student member of Institute of Electrical and Electronics Engineers (IEEE), International Society for Optical Engineers (SPIE), and *Optical Society of America* (OSA).

Amir Hosseini (S'05–M'13) received the B.Sc. degree in electrical engineering in 2005 from Sharif University of Technology, Tehran, Iran, the M.Sc. degree in electrical and computer engineering in 2007 from Rice University, Houston, TX, USA, and the Ph.D. degree in electrical and computer engineering from the University of Texas at Austin, Austin, TX, in 2011.

He has been engaged in research on modeling, design, fabrication and characterization of optical phased array technology, true-time delay lines, and high performance optical modulators. He is a Prince of Wales' scholar in 2011 and received the Ben Streetman Award in 2012, and has authored or coauthored more than 100 peer reviewed technical papers. He is a member of the Optical Society of America and International Society for Optical Engineers. He has been serving as the Principal Investigator for an Air Force Research Laboratory sponsored project on polymer optical modulators since 2012.

Harish Subbaraman (M'09) received the M.S. and Ph.D. degrees in electrical engineering from the University of Texas at Austin, Austin, TX, USA, in 2006 and 2009, respectively. With a strong background in RF photonics and X-band Phased Array Antennas, he has been working on optical true-time-delay feed networks for phased array antennas for the past seven years. Throughout these years, he has laid a solid foundation in both theory and experimental skills. His current research areas include printing and silicon nanomembrane-based flexible electronic and photonic devices, polymer photonics, slow-light photonic crystal waveguides, carbon nanotube and silicon nanoparticle nanofilm-based ink-jet printed flexible electronics, and RF photonics. He has served as a PI on eight SBIR/STTR Phase I/II projects from National Aeronautics and Space Administration, Air Force, and Navy. He has more than 70 publications in refereed journals and conferences.

Shiyi Wang , received the B.S. and M.S. degrees in optics from Harbin Institute of Technology, Harbin, China, in 2008 and 2010, respectively. He is currently working toward the Ph.D. degree in electro-optics at the University of Dayton, Dayton, OH, USA. His research mainly focuses the design, simulation, and characterization of subwavelength metallic structures, including RF antennas for photonic applications and metasurfaces for complex optical field engineering in optical and infrared regions.

Qiwen Zhan (M'00–SM'11) received the B.S. degree in physics (optoelectronics) from the University of Science and Technology of China, Hefei, China, in 1996 and the Ph.D. degree in electrical engineering from the University of Minnesota, Minneapolis, MN in 2002. He is a Professor of electro-optics and electrical & computer engineering at the University of Dayton, Dayton, OH, USA. He is the PI at the Nano Electro-Optics Laboratories at the University of Dayton and serves as the Managing Director of the University of Dayton Fraunhofer Research Center, Dayton. Currently, his research mainly focuses on utilizing modern nanofabrication tools to achieve comprehensive spatial engineering of light wave properties (such as polarization, intensity, and phase) and subsequently manipulate the light matter interactions on the nanometer scale with these engineered optical fields. The localized light matter interactions are exploited in various applications, including the development of new nanoscale imaging capabilities, novel nanophotonic and plasmonic devices, biophotonics, nanomaterials characterization, and metrology. He has received four US patents, published more than 80 peer reviewed journal articles, delivered many invited talks at major international conferences, and given invited lectures and seminars around the world. He is a Topical Editor of Applied Optics, short course instructor for the Optical Society of America (OSA) and The International Society for Optical Engineers (SPIE) on Nanophotonics, fellow of the SPIE, a fellow of the OSA, and a member of the Annual Antenna Applications Symposium.

Jingdong Luo received the Ph.D. degree in chemistry from Wuhan University, Wuhan, China, in 2000. He is the Senior Research Scientist at the Department of Materials Science and Engineering, University of Washington, Seattle, WA, USA. He is the Cofounder of Soluxra, LLC, Seattle, aims at producing cutting-edge high-performance functional materials and their hybrid systems to fulfill the diverse customer needs for applications in telecommunication, optical computing, sensing, and clean energy technologies. He led the recent development of a series of high-performance electro-optic polymers (such as SEO100, SEO125, SEO250, and SEO500) as new generation high-performance (r_{33} values up to 250 pm/V) photonic polymer products. He has dedicated more than ten years of research experience in the field of organic photonics and electronics. He has coauthored more than 160 research papers and texts with numerous scientific citations ($>$7000 times), and holds 13 patents on organic functional materials for optoelectronics and photonics. His major scientific achievements include supramolecular engineering of organic nonlinear optical materials for low-driven voltage modulators, efficient pyroelectric poling of organic/polymeric dielectric materials, high-performance electro-optic polymers for CPU CMOS and silicon photonic platforms, and aggregation-induced emission mechanism for organic light-emitting diode and sensing applications.

Alex K.-Y Jen received the Ph.D. degree from the Department of Chemistry, University of Pennsylvania, Philadelphia, USA, in 1984.

He is the Boeing-Johnson chair professor at the Materials Science and Engineering Department of the University of Washington, Seattle, WA, USA. His research focuses on utilizing molecular, polymeric and biomacromolecular self-assembly to create ordered arrangement of organic, inorganic and hybrid functional materials for photonics, optoelectronics, nanomedicine, and nanotechnology. He has coauthored more than 500 papers, given more than 350 invited presentations. His work has been widely cited for more than 18,000 times and with a H-index of 71. He is also a coinventor for more than 50 patents and invention disclosures.

For his pioneering contributions in organic photonics and electronics, Dr. Jen has been elected as a fellow by Materials Research Society, American Chemical Society, American Association of the Advancement of Science, Optical Society of America, International Society of Optical Engineering, and by Polymeric Materials Science & Engineering Division of ACS. He has also been elected as a member of Washington State Academy of Sciences in 2011.

Ray T. Chen (M'91–SM'98–F'04) received the B.S. degree in physics from National Tsing-Hua University in 1980, Hsinchu City, Taiwan and the M.S. degree in physics in 1983, and the Ph.D. degree in electrical engineering in 1988, both from the University of California, Oakland, CA, USA. He holds the Cullen Trust for Higher Education Endowed Professorship at University of Texas at Austin, TX, USA and the Director of Nanophotonics and Optical Interconnects Research Lab within the microelectronics research center. He is also the Director of a newly formed AFOSR MURI-Center involved faculty from Stanford, University of Illinois at Urbana–Champaign, Rutgers for Silicon Nanomembrane. He joined UT Austin as a faculty to start optical interconnect research program in the Electrical and Computer Engineering Department in 1992. Prior to his UT's professorship, he was a Research Scientist, Manager and the Director of the Department of Electro-optic Engineering in Physical Optics Corporation in Torrance, Torrance, CA, USA, from 1988 to 1992.

He also served as the CTO/Founder and the Chairman of the board of Radiant Research from 2000 to 2001, where he raised 18 million dollars A-Round funding to commercialize polymer-based photonic devices. He also serves as the Founder and the Chairman of the board of Omega Optics Inc. since its initiation in 2001. Over 5 million dollars of research funds were raised for Omega Optics. His research work has received with 110 research grants and contracts from such sponsors as Department of Defense, National Science Foundation, Department of Energy, National Aeronautics and Space Administration, National Institutes of Health, Environmental Protection Agency, the State of Texas, and private industry. The research topics are focused on three main subjects: 1. Nanophotonic passive and active devices for optical interconnect and biosensing applications, 2. Polymer-based guided-wave optical interconnection and packaging, and 3. True time delay wide band phased array antenna. Experiences garnered through these programs in polymeric material processing and device integration are pivotal elements for the research work conducted by his group.

Dr. Chen's group at UT Austin has reported its research findings in more than 650 published papers including more than 85 invited papers. He holds 20 issued patents. He has Chaired or been a program-committee member for more than 90 domestic and international conferences organized by IEEE, The International Society of Optical Engineering (SPIE), Optical Society of America (OSA), and PSC. He has served as an editor, coeditor or coauthor for 22 books. He has also served as a Consultant for various federal agencies and private companies and delivered numerous invited talks to professional societies. He Chen is a fellow of the OSA and SPIE. He received the 1987 UC Regent's dissertation fellowship and of 1999 UT Engineering Foundation Faculty Award for his contributions in research, teaching, and services. He received IEEE Teaching Award in 2008. Back to his undergraduate years in National Tsing-Hua University, he led a university debate team in 1979 that received the national championship of national debate contest in Taiwan. Forty-four students have received the EE Ph.D. degree in his research group at UT Austin.